Forward and Adjoint Modeling of Three Viscoacoustic Equations Based on Rheological Models Using DEVITO

Laian de M. Silva[1*], Peterson Nogueira[1,2], Laue R. de Jesus[1]
[1]SENAI/CIMATEC University Center; [2]Federal University of Bahia, INCT-GP; Salvador, Bahia, Brazil

Disregarding the effect of seismic signal attenuation in gas and hydrocarbon zones leads to a final image with low resolution. However, a range of equations called viscoacoustics overcome such limitations. We use three second-order equations based on Maxwell, Kelvin-Voigt (KV), and Standard Linear Solid (SLS) models. We analyze the dissipation and dispersion effects on each of them through seismograms. We also perform Reverse Time Migration (RTM) using the exact adjoint operators (Q-RTAM). All numerical experiments were implemented using Devito - a domain-specific language (DSL) and code generation framework to design highly optimized finite difference kernels for use in inversion methods.
Keywords: Viscoacustic Equations. Domain-Specific Language. DEVITO. Seismic Attenuation.

Introduction

The seismic signal suffers a mechanical energy loss when propagating through the rock. Such loss is reflected in the attenuation phenomenon. The attenuation of the seismic signal is present in the seismograms due to the dispersive and dissipative effect of the signal [1-3]. The dispersive effect causes the dephasing of particular frequency contents, and the dissipation reduces the signal's amplitude. Both combinations cause significant signal distortion when such effects are not considered.

Although several theoretical models, mainly in the frequency domain, have been developed to describe the effect of attenuation, the ones with the best physical meaning are those based on Rheological models composed of a series of relaxation mechanisms [2]. Of this range of rheological models, three deserve to be highlighted. They are Maxwell, Kelvin-Voigt (KV), and Standard Linear Solid (SLS) because they are easy to implement. The Maxwell model consists of a series combination of springs (responsible for the elastic behavior of the material) and dashpot (attenuation element). In this model, the force/stress applied to the elements are equivalent, changing only the response of each element, also known as strain, which is more significant in the spring than in the dashpot.

As a consequence of this behavior, its quality factor (Q) is directly proportional to the frequency, with the most outstanding damping occurring at low frequencies [4]. The Kelvin-Voigt Model represents a parallel combination of spring and dashpot. The strain in both elements is the same; however, each element's force or stress is different. Consequently, its quality factor Q is inversely proportional to the frequency, and the attenuation is more potent at higher frequency contents. Consequently, its quality factor is inversely proportional to the frequency, and the attenuation is more substantial at higher frequency contents. The stress-strain relationship obtained from this model is of the convolutional temporal type, which requires recording the wave fields in each. However, this temporal convolution can be replaced by introducing an auxiliary memory variable [4].

The present work compares wave fields, seismograms, and RTAM images for geological media of different complexities. The equations based on the SLS, Kelvin-Voigt, and Maxwell models are well-defined in the works of Carcione and colleagues [5], Deng and colleagues [6], Gardner and colleagues [7], and Carcione [4]. We implement all equations using Devito, a DSL used to solve

Received on 17 December 2022; revised 6 January 2023.
Address for correspondence: Laian de M. Silva. Avenida Orlando Gomes, S/N, Salvador, Bahia, Brazil. Zipcode: 41650-010. E-mail: laianufba@gmail.com.

J Bioeng. Tech. Health 2023;6(Suppl.1):6-13.

modeling and seismic inversion problems in a high-performance computational environment [8, 9].

Forward and Adjoint Modeling Equations

The construction of mechanical models is based on two elements (springs and dashpots) connected in parallel or a combination of series and parallel. The spring represents the elastic behavior, whereas the dashpot (represented by a cylindrical piston filled with viscous liquid) denotes the dampening behavior.

The viscoacoustic equations based on rheological models originated from the stress-strain relationship.

$$\sigma = \frac{\partial \psi}{\partial t} * \varepsilon = \psi * \frac{\partial \varepsilon}{\partial t}, \tag{1}$$

σ is the stress, ε is the deformation, and ψ is the relaxation function. Moreover, we have the following relation:

$$\frac{\partial \varepsilon}{\partial t} = \nabla \cdot \mathbf{v}, \tag{2}$$

with v being obtained by the motion equation:

$$\frac{\partial \mathbf{v}}{\partial t} = \frac{1}{\rho} \nabla \sigma, \tag{3}$$

in which v is the particle velocity, and ρ is the density.

Maxwell Model

The relaxation function for the Maxwell model is defined as:

$$\psi = M_U e^{(-t/\tau)} H(t) \tag{4}$$

in which M_U is the elasticity constant of the unrelaxed spring, H(t) is the Heaviside function, and $\tau = \eta / M_U = \omega_0 Q$ is the relaxation time (η is the viscosity and Q is the quality factor). From Equation 1 with some operations, we obtained the equations system:

$$\begin{cases} \frac{\partial p}{\partial t} + \kappa \nabla \cdot \mathbf{v} + \frac{\omega_0}{Q} p = \int S(\mathbf{x}_s, t) \\ \frac{\partial \mathbf{v}}{\partial t} + \frac{1}{\rho} \nabla p = 0, \end{cases} \tag{5}$$

in which κ is the Bulk modulus and $\omega_0 = 2\pi f_0$ is the angular frequency (f_0 is the dominant frequency). Differentiating about time the first Equation of system 5 and substituting the second in the first, there is as follows:

$$\frac{\partial^2 p}{\partial t^2} - \kappa \nabla \cdot \frac{1}{\rho} \nabla p + \frac{\omega_0}{Q} \frac{\partial p}{\partial t} = S(\mathbf{x}_s, t) \tag{6}$$

The adjoint-state method [10] was used to computation the adjoint equation of the forward modeling operator. Applying the adjoint operation in Equation 6, we have the following:

$$\frac{\partial^2 q}{\partial t^2} - \nabla \cdot \frac{1}{\rho} \nabla \kappa q + \frac{\omega_0}{Q} \frac{\partial q}{\partial t} = -\Delta d \tag{7}$$

Kelvin-Voigt Model

The relaxation function to the KV model is determined as:

$$\psi = M_R H(t) + \eta \delta(t), \tag{8}$$

in which M_R is the elasticity constant of the relaxed spring, η is the viscosity, H(t) and δ(t) are the Heaviside and Dirac delta functions, respectively. Once more, starting from Equation 1, using the relaxation function (Equation 8) and following some steps:

$$\begin{cases} \frac{\partial p}{\partial t} + \kappa \nabla \cdot \mathbf{v} - \eta \nabla \cdot \frac{1}{\rho} \nabla p = \int S(\mathbf{x}_s, t), \\ \frac{\partial \mathbf{v}}{\partial t} + \frac{1}{\rho} \nabla p = 0. \end{cases} \tag{9}$$

in which $\eta = \tau \kappa$ with $\tau = (\omega_0 Q)^{-1}$, where κ, η and τ are the Bulk moduli, viscosity, and relaxation time, respectively. Differentiating regarding time, the first Equation of system 9 and substituting the equation of motion, we arrive at:

$$\frac{\partial^2 p}{\partial t^2} - \kappa \nabla \cdot \frac{1}{\rho} \nabla p - \eta \nabla \cdot \frac{1}{\rho} \nabla p = S(\mathbf{x}_s, t) \tag{10}$$

After applying the adjoint-state method in Equation 8, we obtain:

$$\frac{\partial^2 q}{\partial t^2} - \nabla \cdot \frac{1}{\rho} \nabla \kappa q + \nabla \cdot \frac{1}{\rho} \nabla \eta q = -\Delta d \tag{11}$$

SLS Model

The SLS model is the most realistic, consisting of a KV model connected in series with a spring. The relaxation function of this model is defined by

$$\psi = M_R\left[1-\left(1-\frac{\tau_\varepsilon}{\tau_\sigma}\right)e^{-t/\tau_\sigma}\right]H(t) \tag{12}$$

Thus, starting with Equation 1, using Equation 10, and following some steps, there are as follows:

$$\begin{cases} \frac{\partial^2 p}{\partial t^2} - \kappa(1+\tau)\nabla\cdot\frac{1}{\rho}\nabla p + r_p = S(\mathbf{x}_s,t) \\ \frac{\partial r_p}{\partial t} - \frac{\tau}{\tau_\sigma}\rho\nabla\cdot\frac{1}{\rho}\nabla p + \frac{1}{\tau_\sigma}r_p = 0 \end{cases} \tag{13}$$

Where ρ(x) is the density at position x, $\kappa(x)$ is the Bulk modulus, $\mathsf{v} = v(x,t)$ is the particle velocity vector, and $S = S(x_s,t)$ is the source at position x_s. The symbol $*$ represents a convolution operation, which describes the dissipation mechanism in a viscoacoustic medium in Equation 1. $\tau = \tau_\varepsilon/\tau_\sigma - 1$ represents the magnitude of Q. τ_ε and τ_σ are, respectively, the relaxation time stress and strain, given by:

$$\tau_\sigma = \frac{\sqrt{Q^2+1}-1}{2\pi f_0 Q} \quad and \quad \tau_\varepsilon = \frac{\sqrt{Q^2+1}+1}{2\pi f_0 Q} \tag{14}$$

Applying the adjoint-state method in Equation 11:

$$\begin{cases} \frac{\partial^2 q}{\partial t^2} - \nabla\cdot\frac{1}{\rho}\nabla(1+\tau)\kappa q + \nabla\cdot\frac{1}{\rho}\nabla\rho r_q = -\Delta d, \\ \frac{\partial r_q}{\partial t} + \frac{\tau}{\tau_\sigma}q - \frac{1}{\tau_\sigma}r_q = 0 \end{cases} \tag{15}$$

Numerical Experiments

Two-Layer Model

The two-layer model (Figure 1) is used to show the stability of the viscoacoustic modeling for a medium with high-velocity contrast and Q factor and to highlight the reflection and transmission phenomena in Figure 6.

Figure 2a shows a modeled seismogram with a source in the center at the surface. According to the reflection indicated by the red arrow, a substantial drop in amplitude occurs in all viscoacoustic equations. However, the SLS model is the one that has the lowest loss, especially the Maxwell model, which ends up with an almost imperceptible reflection. Therefore, we compared the traces taken at the 1 km position to more accurately observe the effects observed in the seismograms (Figures 2a and 2b). In this image, the green trace has a sizeable temporal displacement concerning the others, indicating that the SLS models have a strong dispersion. Still analyzing the green trace, there is also a marked loss of amplitude concerning the reference acoustic. On the other hand, the KV and Maxwell EVAs showed only energy dissipation, with Maxwell being extremely sensitive to low Q factor values.

Figure 1. Two-layer model parameters. Top layer: v =1800 m/s and Q = 30. Bottom layer: v = 3000 m/s and Q = 100.

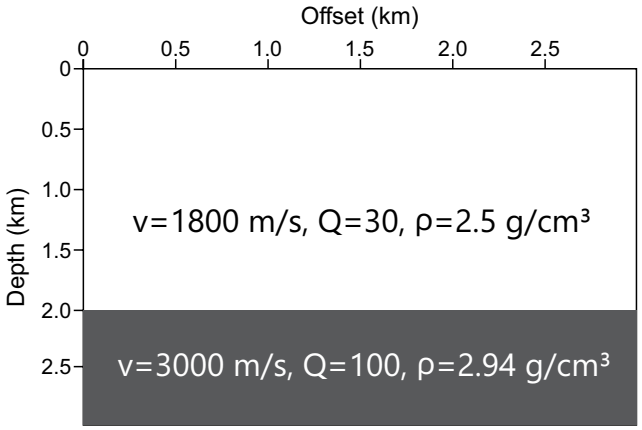

Figure 2c presents the time instants of a wave field propagated up to 0.5 s time. At first glance, it is worth noting that the generated wavefronts with the Maxwell and KV equations present more evident energy dissipation than those of the SLS. Therefore, we took a trace at the 1.5 km offset (Figure 2c) to the wavefront of all equations and put them together in a comparison (Figure 2d). Observing these comparisons, we concluded that the green dashed line representing the SLS model is the only one that presents a phase shift concerning the acoustic case, regardless of the order of the equation used.

Figure 2. Seismogram comparisons, for two layer model, between acoustic a viscoacoustic cases (a) and vertical traces comparison at 1 km (b) Snapshots comparison, for two-layer model, between acoustic and viscoacoustic cases at instances of 0.5s (c) and vertical traces comparison at 1.5 km (d).

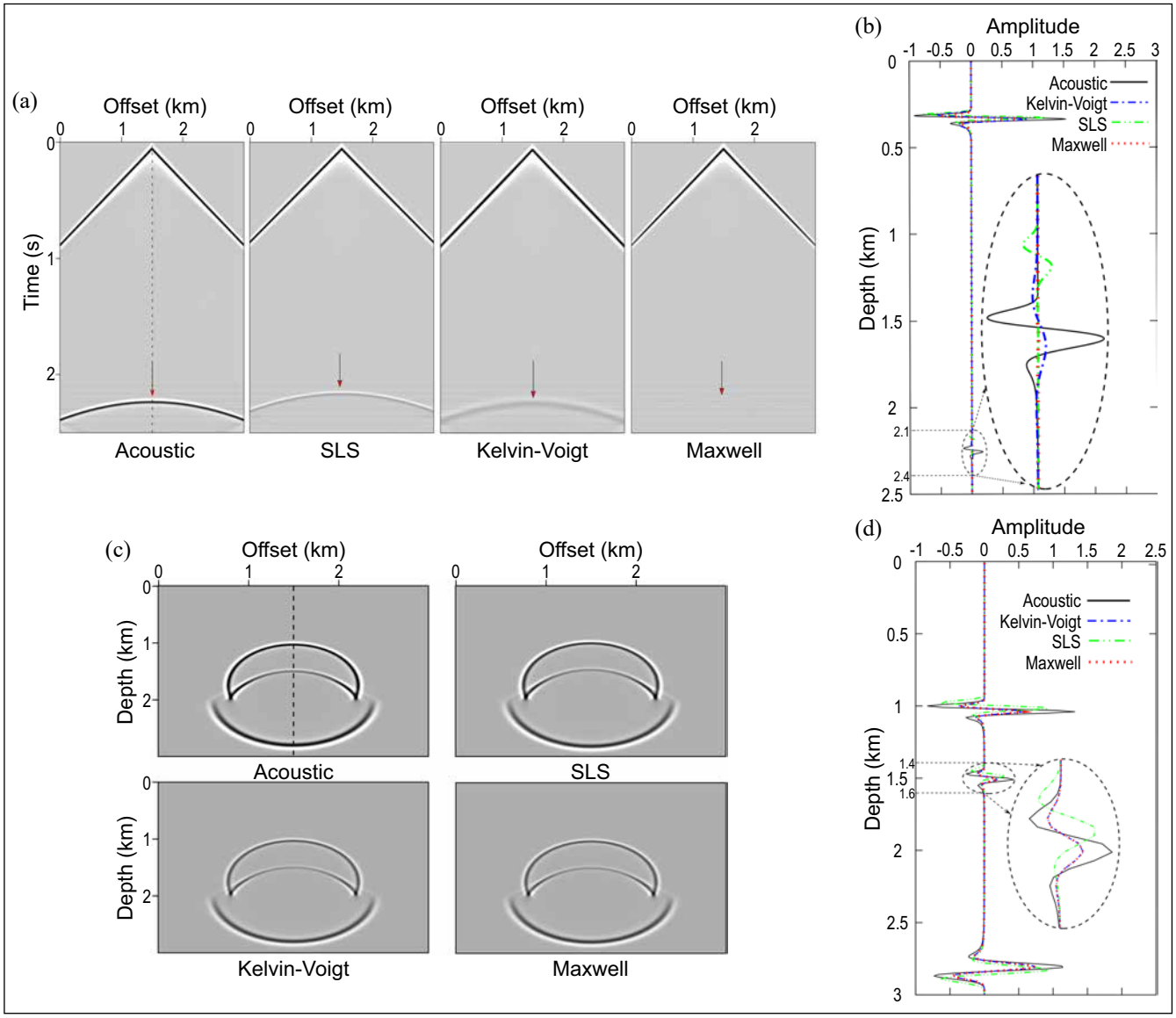

Marmousi

Figure 3a shows the velocity model. The values vary from 1,500 m/s to 5,500 m/s. And the Q model was calculated by empirical equation $Q = 3.516 \times v^{2.2} \times 10^{-6}$ [8]. Finally, we obtained the density model using the Gardner relation [11]. In addition, we calculated an approximation of reflectivity (Figure 2b). These models have 9.2 × 3 km 2 and were discretized with nx = 369 and nz = 375 samples in a mesh of $\Delta x = 25$ m and $\Delta z = 8$ m. The recording time was 4 s, with a frequency peak of 12 Hz, considering 5716 samples at a sampling interval $\Delta t = 0.7$ ms.

We performed numerical simulations for the seismogram with the source located at 4.7 km and receivers scattered on the surface. The arrows in Figure 4a show a decrease in the amplitudes of seismic events. Analyzing the central region of the seismograms in the time interval from 1.5 to

Figure 3. Marmousi model: velocity (a) and reflectivity (b).

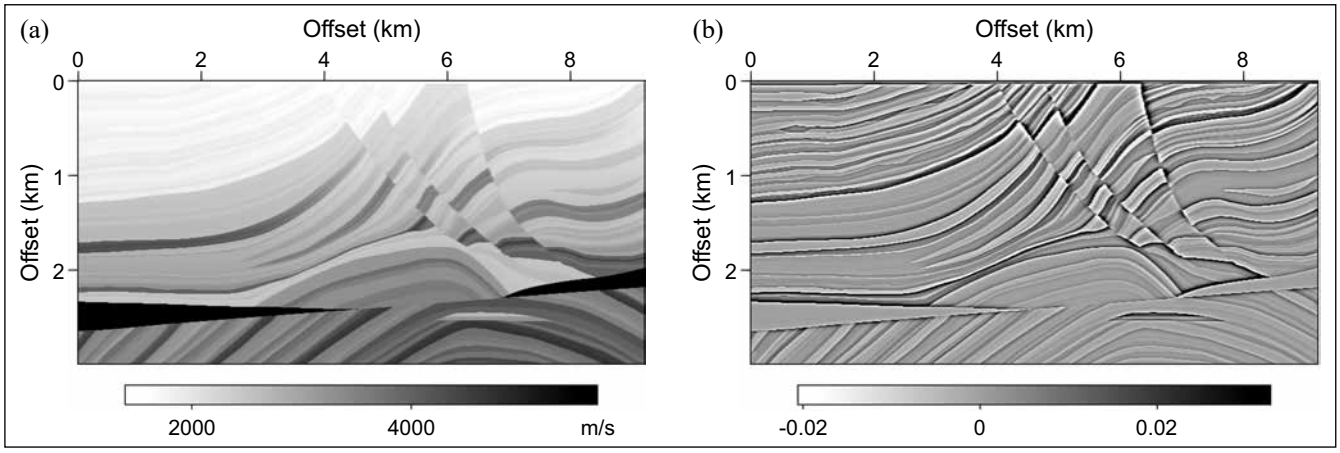

2.5 s presents a more significant attenuation than the other regions, mainly for the Maxwell and KV viscoacoustic equations. Figure 4c ahows the traces taken at 3.75 km offset. Examining the green trace in the SLS viscoacoustic equation, we observe that a temporal displacement does not occur in the remaining traces, indicating that only phase dispersion occurs for this equation.

Figure 5 presents the Q-RTAM results for the SLS, Kelvin-Voigt, and Maxwell models. Figures show that the SLS image is much superior to KV and Maxwell. This is due to equations based on SLS models better compensating for the signal dispersion, something that is less noticeable in the other equations than has already been seen. KV, on the other hand, presents a significantly better result than Maxwell due to the dissipative effect in Maxwell being stronger at lower frequencies, which is where most of the frequency content of the seismic is represented.

Gas Chimney

The Gas Chimney constitutes a minor clipping of the BP model [12]. Figure 6a and Figure 6b

Figure 4. Marmousi model: seismograms comparison among acoustic, SLS, KV, and Maxwell equations (a) and traces comparison at 3.75 km (b).

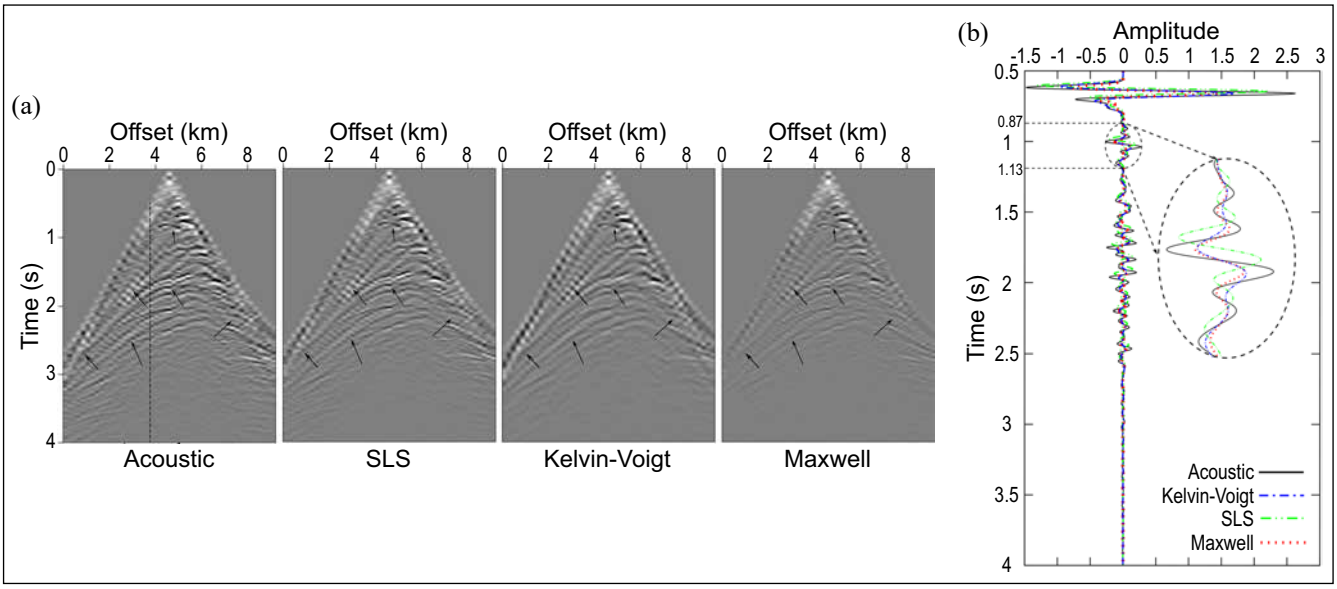

illustrate the velocity and reflectivity, respectively. The density and Q factor were calculated by the Gardner relation [13] and empirical equation [8]. These models have $9.995 \times 4km^2$ discretized with nx = 995 and nz = 402 samples.

Figure 7a shows all the seismograms for the analyzed viscoacoustic equations. The Gas Chimney model has a low Q factor anomaly in the upper central part of the model (Figure 7a). The effect is notable in seismograms, presenting significant energy loss, mainly for the Maxwell model. Analyzing the red dashed circle, we notice that the dissipative effect is not as strong as the region for the longer times indicated by the arrows.

Furthermore, the SLS equation's velocity phase dispersion effect exists beyond amplitude reduction, which causes seismic pulse distortion. The traces for the equations based on the Maxwell and KV rheological models show the dissipative effect (Figure 7). However, they are not displaced, characterizing the non-occurrence of the dispersive effect because these viscoacoustic equations do not consider the dispersion phenomena.

Figure 8 shows the result for the Q-RTAM for the gas chimney model. In this figure, the behavior seen in the Marmousi is repeated, where the SLS presents a better result, and it is possible to observe the characteristics of the model in the region of the chimney of the Q factor. The KV also presents a better resolution, mainly in the chimney region.

Figure 5. Marmousi model: Q-RTAM for SLS, Kelvin-Voigt and Maxwell rheological model.

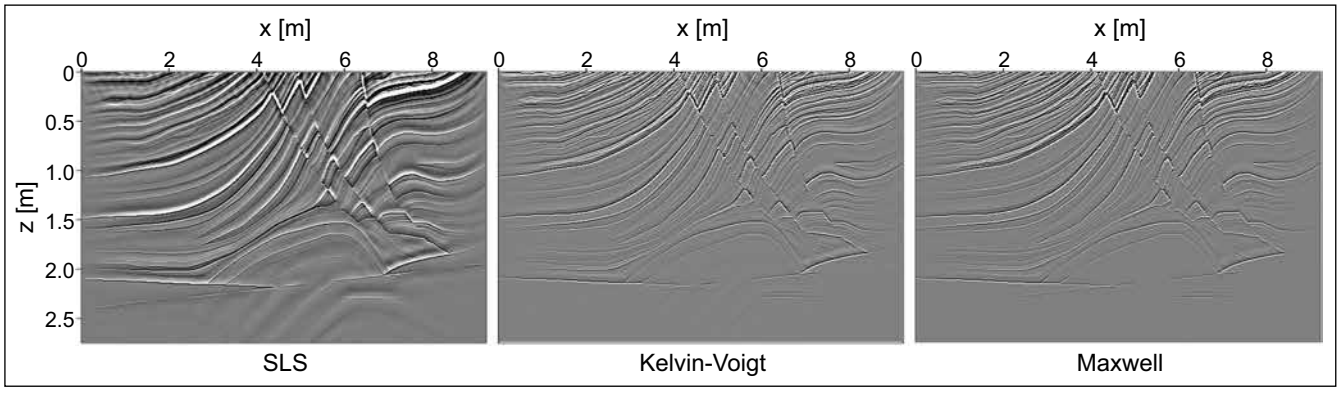

Figure 6. Gas chimney model: velocity (a); reflectivity (b).

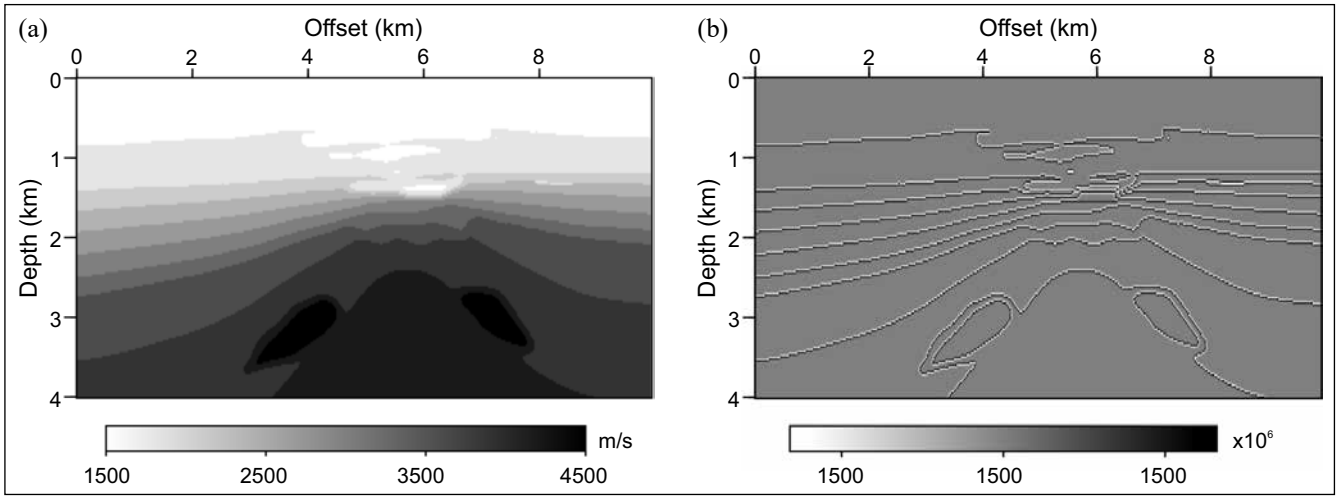

Conclusion

We performed physical-numerical experiments considering velocity, quality factor, and density models with different complexities, explaining in detail the behavior and characteristics of each equation. Unlike the equations based on the Maxwell and KV models, the SLS equations can reasonably simulate the energy dissipation and phase dispersion phenomena in the forward modeling stage.

Acknowledgments

This study was financed by the project PIE00005/2016 of Infrastructure Edictal of FAPESB 003/2015 and was financed in part by the Coordenação de Aperfeiçoamento de Pessoal de Nível Superior-Brazil (CAPES)-Finance Code 001.

Figure 7. Gas chimney model: seismogram comparisons between acoustic, SLS, KV, and Maxwell equations (a), and traces comparison at 3.75 km (b).

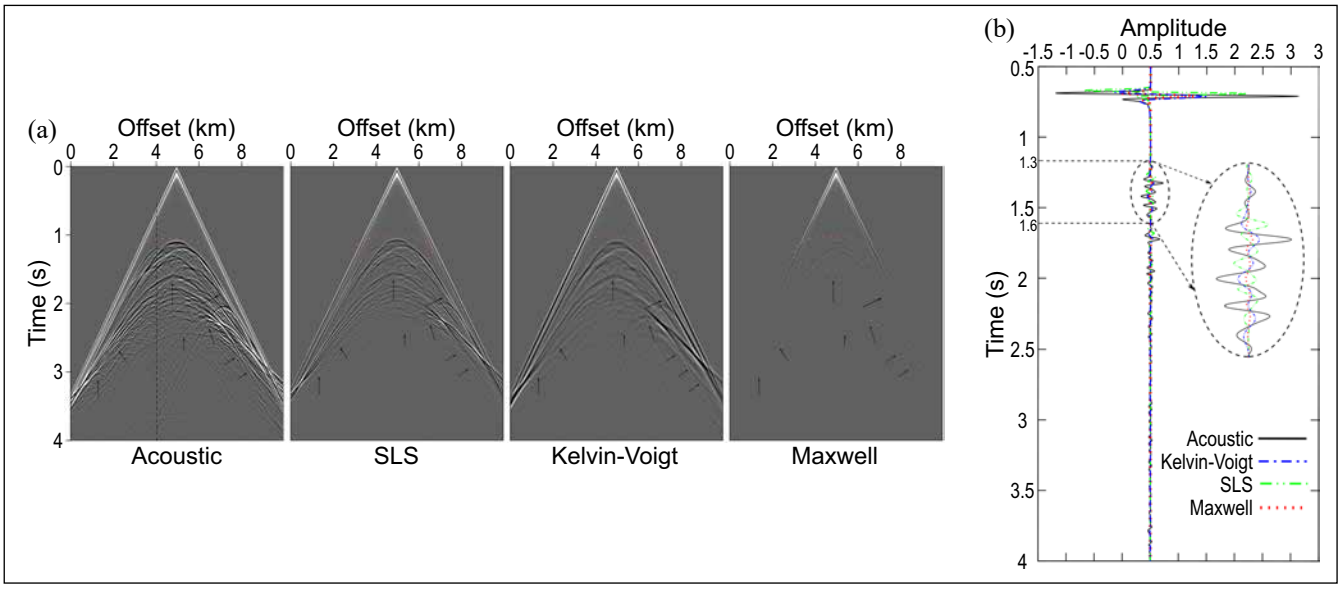

Figure 8. Gas chimney model: Q-RTAM for SLS, Kelvin-Voigt and Maxwell rheological model.

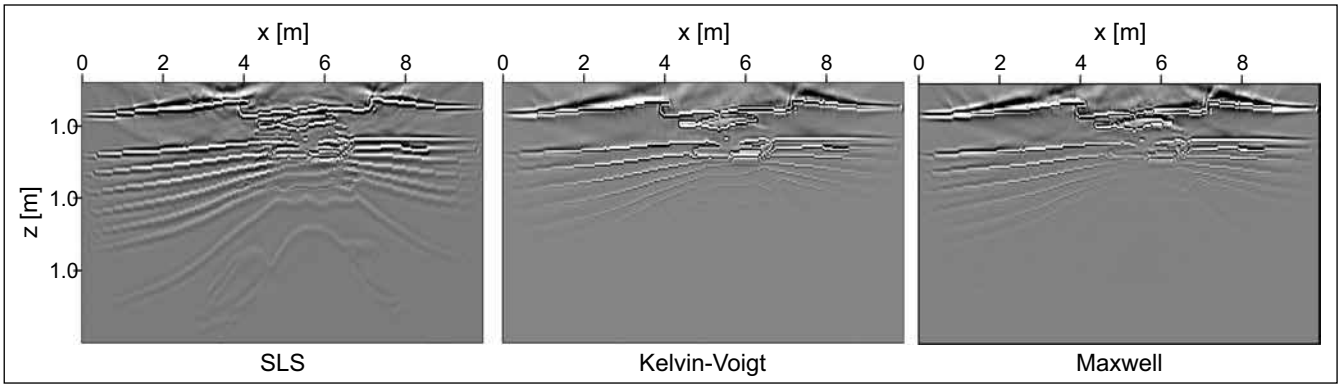

References

1. Walcott R. Flexural rigidity, thickness, and viscosity of the lithosphere, Journal of Geophysical Research. 1970;75(20):3941–3954.
2. Schiessel H, Metzler R, Blumen A, Nonnenmacher T. Generalized viscoelastic models: Their fractional equations with solutions. Journal of Physics: Mathematical and General 1995;28(23):6567.
3. Robertson JO, Blanch JO, Symes WW,.Viscoelastic finite-difference modeling, Geophysics. 1994;59(9):1444–1456.
4. Carcione JM, Kosloff D, Kosloff R. Wave propagation simulation in a linear viscoelastic medium. Geophysical Journal International 1988;95(3):597–611.
5. Carcione JM. Wave Fields in Real Media: Wave Propagation in Anisotropic, Anelastic, Porous, and Electromagnetic Media, Elsevier, 2014.
6. Bai JD, Yingst R, Bloor, Leveille J. Viscoacoustic waveform inversion of velocity structures in the time domain. Geophysics 2014;79:R103–R119.
7. Ren Z, Liu Y, Zhang Q. Multiscale viscoacoustic waveform inversion with the second generation wavelet transform and adaptive time–space domain finite-difference method. Geophysical Journal International 2014;197(2):948–974.
8. Kukreja N et al. High-level python abstractions for optimal checkpointing in inversion problems. arXiv preprint arXiv 2018. 1802.02474.
9. Louboutin M et al. Devito: An embedded domain-specific language for finite differences and geophysical exploration. arXiv 2018. preprint arXiv:1808.01995.
10. Plessix R-E. A review of the adjoint-state method for computing the gradient of a functional with geophysical applications. Geophysical Journal International 2006;167(2):495–503.
11. Gardner G, Gardner L, Gregory A. Formation velocity and density—the diagnostic basics for stratigraphic traps. Geophysics 1974;39(6):770–780.
12. Billette F, Brandsberg-Dahl S. The 2004 bp velocity benchmark. 67th EAGE Conference & Exhibition, European Association of Geoscientists & Engineers 2005;Supl–1.
13. Deng F, McMechan GA. True-amplitude prestack depth migration. Geophysics 2007;72(3):S155–S166.